Multi-objective Pareto Optimal Power Quality Improvement in Distribution Systems

Anushree Roy[1]*, Sudipta Debnath[2] , Yadala Pavankumar [3]

[1] Department of Electrical Engineering, B.P.Poddar Institute of Management and Technology, Kolkata 700052, India

[2]Department of Electrical Engineering, Jadavpur University, Kolkata 700032, India

[3]School of Electronics and Computer Science, University of Southampton, SO17 1BJ, UK

E-mail:anushreebppimt@gmail.com

Keywords: Power quality improvement, Electric Spring, Multi objective optimisation, Unbalance minimisation, Power quality factor

Abstract: The present study proposes a multi-objective optimized Electric Spring (ES) operation to improve the voltage regulation and overall power quality in a distribution system. A suitable controller has been designed for the ES implementing the Multi-objective artificial cooperative search (MOACS) optimization algorithm. The objectives are to enhance the system power factor, regulate the critical load voltage, and minimize the neutral current. The proposed technique provides satisfactory results with intermittent energy source also. The performance of MOACS has been compared with particle swarm optimization (PSO) and harmony search (HS) algorithms. It has been observed that the improvement in power factor and reduction of neutral current is much more in MOACS compared to PSO and HS. The power quality factors obtained with PSO are 0.9136, 0.9257, and 0.9146 for three different sets of loads, whereas, with HS, these values are 0.9072, 0.9324, and 0.8985. The same index improves to 0.9465, 0.9392, and 0.9307 with MOACS, which proves the efficacy of MOACS. The validation of the proposed scheme through real-time simulation confirms the reliability of this scheme.

Ethical Compliance: Not applicable.

Data Access Statement: Not applicable.

Conflict of Interest declaration: The authors declare that they have no affiliations with or involvement in any organization or entity with any financial interest in the subject matter or materials discussed in this manuscript.

1. Introduction

The electrical grid nowadays relies heavily on distributed generation (DG) with a significant intrusion of renewable energy sources. The rapid integration of DGs pose problems in power distribution networks. Concerns for power systems include variable load demand in a specific network and intermittent power supply from DGs powered by renewable energy. Demand-side management has been suggested to address the power system stability problems by ensuring a balance between the varying demand and generation [1, 2]. DGs with energy storage devices have also been proposed as a solution to such problems. However, the deficient storage capacity and cost of these devices are major constraints [3]. The penetration of large numbers of inverter-based DGs into the electrical distribution network is a major issue for the deterioration of the quality of the power transferred into the network. Furthermore, the connection of a large number of low voltage, non-linear, and unbalanced loads at the distribution ends worsens the power quality.

One effective solution to address these problems is the implementation of an ES at the low-voltage distribution end. An ES is a voltage source inverter that uses high-speed power electronic switches, DC-link capacitors, or batteries. ES can store energy, maintain the rated voltage, and damp out electrical vibrations [4, 5]. When ES connected in series with a non-critical load (load that can withstand variable voltage), a smart load (SL) is formed. The combination is used as an active power regulator and reactive power compensator connected across the critical load (load that requires a stable voltage) in a network at the distributing end [6]. The characteristics of the ES have been analyzed for both non-linear and linear critical loads. The ES for reactive power compensation has been studied using the linear critical load [7]. Furthermore, the capability of ES has been explored by employing a new control strategy for reducing the total harmonic distortion (THD) with a linear critical load connected to a harmonic-contained source [8]. However, this analysis did not take into account a non-linear critical load. Additional research has been done on the harmonics that are introduced into the system when the ES is linked with a non-linear load [9]

and an innovative control strategy has also been suggested to attain harmonic compensation, power factor correction, and regulation of the critical load voltage. ES has been utilized for stabilizing the voltage and frequency fluctuation in a micro-grid owing to the dynamic load variation and penetration of a large number of renewable energy sources [10]. When intermittent energy sources are present, microgrids that are connected to ES become resilient to variations in voltage and frequency [11-13]. In low voltage networks, three-phase ES is also utilized to achieve direct power management with quick dynamic response and for constant power application across the loads with varying impedances [14-15]. In addition, by regulating the bus voltage with distributed ES, the loss that occurs in microgrids under islanded conditions can be significantly reduced [16]. A suitable controller is necessary so that the ES can operate to meet demand-side requirements. The controller can produce the desired ES output voltage if the ES is managed accurately and optimally. Consequently, the overall performance of the system improved. The main performance criteria of the controller suggested in [14] are high accuracy and speed. The controller's response time for damping out both active and reactive power is less than 2 ms. The authors in [15] examined two control strategies for the ES, viz., closed-loop proportional-integral (PI) control and direct open-loop control. The findings from the simulation and experimentation show that the transient response of ES with the open-loop controller has a higher output deviation but achieves faster convergence with instant settling time and less space complexity. Conversely, with PI controller, the settling time rises to 0.15 s with less steady-state output deviation. The space complexity of this PI controller is more than the open loop controller. The predictive control optimization suggested in [16] evaluates the performance to reduce voltage variation by taking into account both computational speed and accuracy. The control algorithm is straightforward and has less computational time with a communication delay of 1.5 s. However, the accuracy of the results gets impacted by the model's linearization.

The optimization strategy of the controller plays a crucial role. Particle swarm optimization (PSO) and genetic algorithm (GA) techniques for single-objective functions have been used in the majority of the work done so far in this field. Optimal power flow, neutral current, cost, and bus voltage variation have been optimized using these techniques [17-20]. Simulation results obtained in [19] show that the

optimization technique requires an average time of 1.4 min to 1.8 min to solve the optimization problem using a high-end processor. The continuous genetic algorithm-based controller for ES proposed in [20] has a computational time of 350.18 s for execution in each step. The computational time can be reduced only by using super-computers. The algorithm can efficiently give an optimal solution with increased complexity. However, during the functioning of a power system in the real world, several objectives must be achieved to maintain the efficiency and quality of the power handled by the system. Multi-objective optimization techniques are gaining popularity as a means of addressing problems with power systems. The performance of a system with hybrid renewable energy sources connected to the grid has been improved in terms of dependability and annual life cycle cost by implementing MOACS [21]. The MOACS algorithm has also been used by the authors in [22] to optimize the DG's functioning and reduce the bus voltage imbalance. Another optimal multi-objective method has been implemented in [23] to achieve reactive power and active power stipulations. However, the work focused much on active power compensation, and unbalanced optimization has not been addressed properly.

Electric power quality in networks with renewable energy sources must be assessed using ES as a compensating technique. Different compensator schemes have been employed to boost the power quality of the network on the distribution side [24]. A static VAr compensator and a static synchronous compensator have been used on a large scale both for VAr compensation and for boosting the quality of power [25]. Although SVC compensates for reactive power, it is incapable of compensating active power. A static synchronous compensator (STATCOM), although compensates for active and reactive power together, compared to it, ES provides better reactive power compensation and voltage regulation [26]. The incorporation of ES to improve the power quality in a dc microgrid has been cited in [27]. Power quality improvement has been reported for different types of non-critical load (NCL) and critical load (CL) by enhancing the power factor, reducing the neutral current, and mitigating harmonics with a properly designed ES controller for a single-phase system [28]. However, the power quality assessment technique for a three-phase, four-wire network coupled with non-linear critical and fluctuating loads has not been properly addressed. Therefore, determining the quality of power transmitted to a distribution network associated

with unbalanced, non-linear, and fluctuating loads is crucial. It may be more convenient to use a single power quality index that shows the network's overall power quality rather than comparing different power quality aspects separately [29].

Different power quality issues in distribution systems and power quality improvement techniques have been discussed in [30-37]. DSTATCOM with a thyristor switched capacitor-thyristor controlled reactor forming a hybrid compensator has been proposed in [30]. The PSO optimized PI controller used for the compensator has been effective in minimizing various power quality issues. The power quality issues have been further addressed in [31] employing optimized FOPID controller-based STATCOM. The authors in [32] determined the rating and location of custom power devices using PSO algorithm along with the minimization of the total harmonic distortion of the system. In grid-connected hybrid renewable energy systems, fuzzy logic controller-based unified power quality conditioner can be used to address power quality concerns such as power factor fluctuations, harmonics, sag, swell, and voltage fluctuation [33]. The study in [34] demonstrated the optimal placement of DGs and DSTATCOMs in IEEE 33-bus system with the objectives to increase the bus voltages, decrease power losses, and maximize economic gains. In order to address the power quality concerns at the PCC and preserve power flow control by reducing the THD at the output, a PI-based maximum power point tracking controller for PV systems and fuzzy controller-based inverter controller have been proposed in [35]. A study on the various applications of FACTS devices, including power quality improvement, congestion control, and stability enhancement, have been conducted in [36]. A review has also been conducted in [37] to investigate the performance of dynamic voltage restorer to address the power quality issues. PSO has been used to optimize reactive power flow and to estimate transmission line parameters in [38] and [39] respectively. Grey Wolf optimization is also powerful in estimating transmission line parameters [40] and is also used in wireless sensor networks [41]. ANN based technique for high quality power supply has been discussed in [42], and a novel mountain gazelle optimizer to solve optimal power flow in a large-scale power system has been addressed in [43]. Control technique for the operation of multiple ESs in an islanded microgrid has been developed in [44]. EVCS demand management and optimal location of EVCS have been discussed in [45, 46]. Optimization

of short term hydrothermal scheduling has been presented in [47]. A control strategy for reactive power compensation of matrix converter has been developed in [48]. The operation of CLC electric spring to achieve voltage stabilization has been studied in [49].

The increasing intrusion of renewable energy sources in the electrical grid has adversely affected the stability of the grid due to their intermittent nature. Moreover, the widespread connection of single phase photovoltaic sources has led to severe voltage fluctuations and imbalance in three phase system. Hence, there is an urgent need to address these issues so that the operation of critical loads connected to the system is not hampered. Traditional methods of improving the voltage profile did not consider other factors that may deteriorate the power quality in the system. The overall improvement of power quality with the application of ES has not been focused, and power quality assessment has not been addressed. Motivated by the need for accurate assessment of power quality during optimized operation of ES, multi-objective power quality improvement has been considered in this paper. It has been established that the MOACS algorithm is a promising algorithm for optimized operation of ES, which results in better power quality by maintaining constant voltage across the critical load. It has been observed that the optimized operation of three phase electric spring for improving the overall power quality utilizing a multi-objective optimization algorithm has not been addressed in the previous works.

The present work introduces a multi-objective power quality (PQ) improvement technique with an optimal Pareto-front solution for a low-voltage network integrated with an ES. Various case studies have been carried out considering unbalanced, non-linear, and sudden changes in the critical load to verify the potency of the technique. The performance of an ES with an intermittent energy source connected to a distributed network has also been studied. The MOACS algorithm has been applied to produce an optimal reference voltage for the ES. The proposed scheme minimizes the unbalanced neutral current, enhances the system power factor, and reduces THD, thereby improving the overall PQ. A single-index power quality factor (PQF) has been used to assesses the PQ improvement. The comparative study with other compensator schemes [50, 51] demonstrates the potency of the proposed scheme.

The primary objectives of the study are as follows:

- To develop an efficient multi-objective algorithm for PQ improvement in a distribution network integrated with an ES.
- To achieve voltage regulation and power factor improvement with unbalanced minimization using the MOACS optimized controller.
- To assess the overall power quality using a single index. Power quality factor (PQF) near 1 indicates improved power quality.
- To observe the effectiveness of the optimized ES, the system has been coupled with an intermittent energy source.
- To compare the potential of the proposed scheme with previous compensator schemes in terms of compensating the reactive power, enhancing the power factor, and minimizing the overall THD.

The remaining part of the paper is organized in the given order. Section 2 describes the operation of the ES as a compensator and voltage regulator. In Section 3, the configuration and modelling of a low-voltage network with ES coupled have been presented. The PQ assessment technique is discussed in Section 4. The controller technology and MOACS algorithm have been presented in Section 5. Section 6 presents the results of simulations performed for different case studies. In Section 7, a comparative analysis on the performance of the proposed scheme with that of other compensator schemes is presented. Section 8 provides some discussions on the present work. Finally, Section 9 summarizes the conclusions of the study.

2. ES as a compensator for distribution network

ES can be considered as a compensator distributed in low-voltage distribution networks, unlike flexible AC transmission devices, which are placed in a centralized mode in a high-voltage transmission network. To improve PQ and hence the performance of the low-voltage distribution system connected either to a stiff source or to an intermittent source, an appropriate compensator needs to be installed. One such special form of compensator is an ES whose control action regulates the voltage and improves the power factor at the receiving end bus where the sensitive load is connected.

2.1. ES as Smart Load (SL)

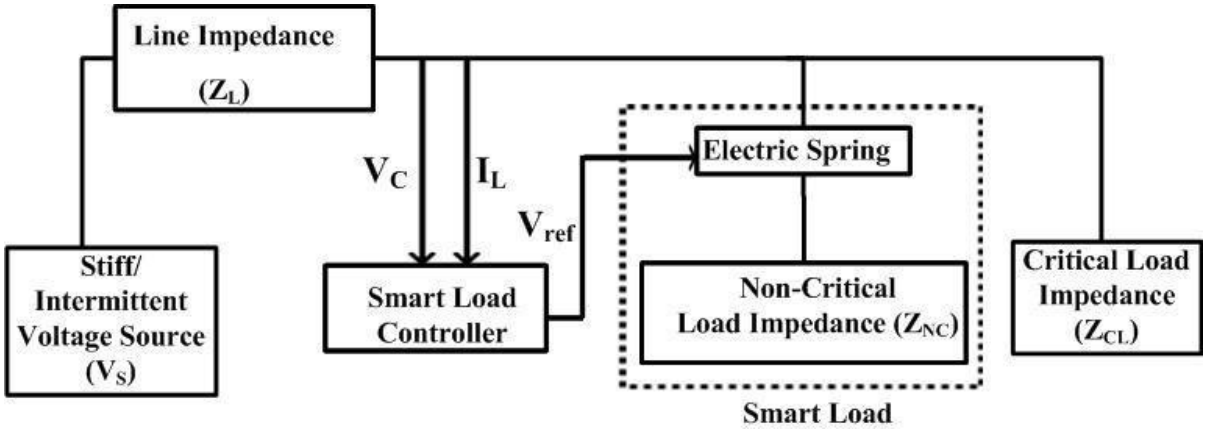

Fig. 1 Schematic diagram of a distribution network connected with ES

The block diagram of a low-voltage distribution system with an ES attached is shown in Fig. 1. The SL comprises an ES in series with a NCL of impedance Z_{NC}. Z_{NC} can endure voltage fluctuations to some extent without causing significant disturbances to the user. The ES with NCL substantially modifies the load into an SL that adaptively consumes energy. The ES, a power electronic device, is capable of generating a compensating voltage V_{ES}, that leads or lags the NCL current I_{NC} to control the NCL voltage V_{NC}. V_{ES} can also alter the magnitude of I_{NC}. This in turn alters the real and reactive powers. The combination of ES and NCL, termed SL, is connected across CL with an impedance Z_{CL}. ES has the potential to maintain a fixed voltage across the sensitive CL at a desired value, reduce power imbalance, and help maintaining the stability of the distribution system. The SL controller generates the reference voltage V_{ref} for the ES, following which the ES generates the voltage V_{ES}. As a result, the NCL voltage, V_{NC} is modulated. Reference voltage, V_{ref}, indicates that the required voltage is maintained across the critical load.

2.2. Working modes of ES

In a distribution system, the AC power source may be stiff or variable. Source voltage variation may occur because of the injection of intermittent sources into the network. Accordingly, the working mode of the ES can be determined. Fig. 2(a) and (b) show the overvoltage and undervoltage scenarios, respectively. In an overvoltage situation, the operation of the ES is in inductive mode, and the ES generates a voltage, V_{ES}, of the correct phase angle so that it becomes perpendicular to V_{NC} and leads I_{NC}. Again, during under-

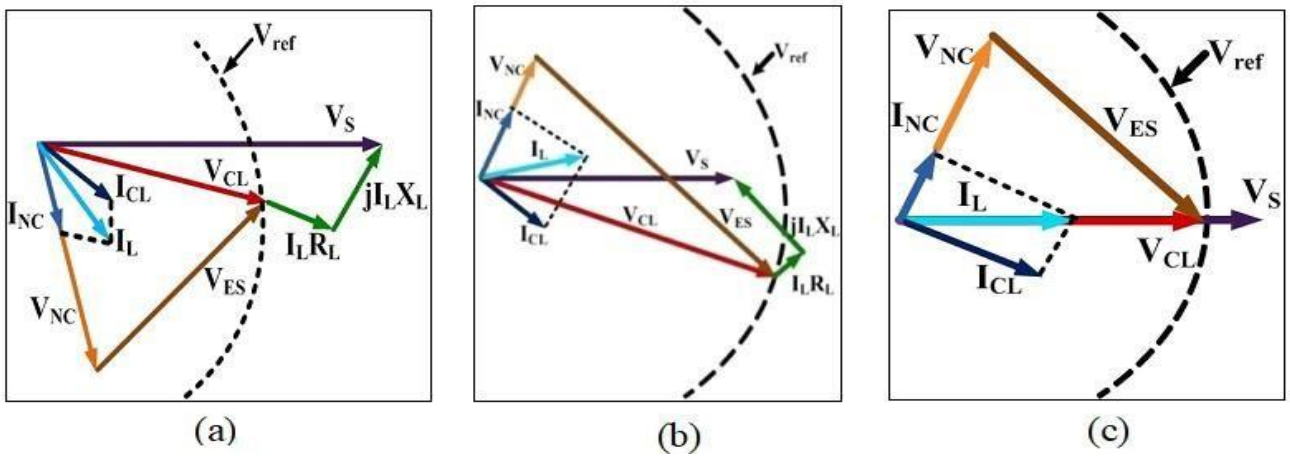

Fig. 2 ES phasor diagram during (a) Over-voltage (b) Under-voltage conditions (c) Power factor improvement

voltage situations, the ES functions in capacitive mode by producing an adequate voltage with the correct phase angle such that I_{NC} leads V_{ES}. V_{ES} again becomes perpendicular to V_{NC}, and as a result, the ES functions as a capacitive VAr compensator when the voltage is low and as an inductive VAr compensator when the voltage is high. Fig. 2(c) illustrates the operation of the ES for power factor improvement. In this case, the line current I_L lies in phase with the supply voltage V_S when the ES produces an appropriate voltage with an appropriate phase angle. Thus, the ES acts as a capacitive VAr compensator by generating a voltage V_{ES} that lags I_{NC}.

3. Circuit configuration and modelling of distribution network with SL

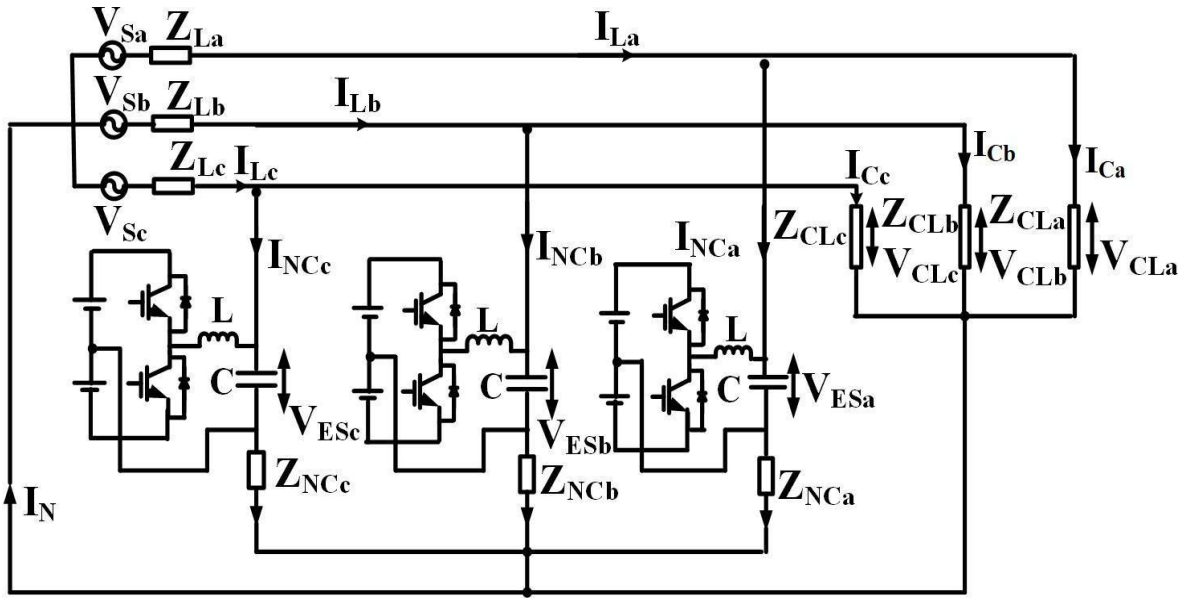

Fig. 3 Circuit diagram of ES

The test system depicted in Fig. 3 has been designed in the MATLAB/ simulink platform to implement the proposed algorithm. The system comprises a 400 kV, 50 Hz, doubly-fed, 300 km long TL, source voltage, three phase ES, NCL and CL loads. V_S represents the source voltage, which has been considered as a stiff source of 220 V. Z_L represents a lumped line impedance of *0.2 + j0.8* Ω per phase. V_{ES} is the voltage generated by the ES for active and reactive power compensation. V_{NC} and V_C are the voltages across NCL and CL, respectively. Z_{NC} of *20* Ω has been considered in the study. Different unbalanced and non-linear Z_{CLs} have been considered with the intention of studying the effectiveness of ES for power quality improvement. I_L, I_N, I_{NC}, and I_C denote the current through the distribution line, neutral path, non-critical load, and critical load respectively.

The three-phase ES modeled herein comprises three single-phase half-bridge inverters with a small regulated DC source. IGBTs with a switching frequency of *20* kHz have been used as switches. The ES has been designed as a voltage-source converter driven by the SPWM technique. The low-pass filter inductor L and capacitor C connected at the output of each inverter leg act as LC filters to produce a smooth output waveform. A low-pass filter inductor of *500* μH and a capacitor of *13.2* μF have been considered for the study. The relationship between the ES voltage and line current has been derived to demonstrate the capacity of the ES for active and reactive power compensation. The three-phase line current is given by:

$$\begin{aligned} I_{La} &= I_{NCa} + I_{CLa} = \frac{V_{CLa} - V_{ESa}}{Z_{NCa}} + \frac{V_{CLa}}{Z_{CLa}} \\ I_{Lb} &= I_{NCb} + I_{CLb} = \frac{V_{CLb} - V_{ESb}}{Z_{NCb}} + \frac{V_{CLb}}{Z_{CLb}} \\ I_{Lc} &= I_{NCc} + I_{CLc} = \frac{V_{CLc} - V_{ESc}}{Z_{NCc}} + \frac{V_{CLc}}{Z_{CLc}} \end{aligned} \quad (1)$$

where, I_{NCa}, I_{NCb}, and I_{NCc} denote the currents through the NCL for phases a, b, and c, respectively. I_{Ca}, I_{Cb}, and I_{Cc} represent the currents in the three phases of the CL. The source voltages V_{Sa}, V_{Sb} and V_{Sc} of the three phases can be expressed as:

$$\begin{aligned} V_{Sa} &= I_{La}Z_{La} + V_{CLa} \\ V_{Sb} &= I_{Lb}Z_{Lb} + V_{CLb} \\ V_{SC} &= I_{Lc}Z_{Lc} + V_{CLc} \end{aligned} \quad (2)$$

Substituting the values of the line currents, I_L from Eq. 1 in Eq. 2, the voltage across the critical load can be expressed as:

$$V_{CLa} = \frac{(V_{Sa} + (Z_{La}/Z_{NCa}) * V_{ESa})}{(1 + Z_{La}/Z_{NCa} + Z_{La}/Z_{CLa})}$$
$$V_{CLb} = \frac{(V_{Sb} + (Z_{Lb}/Z_{NCb}) * V_{ESb})}{(1 + Z_{Lb}/Z_{NCb} + Z_{Lb}/Z_{CLb})} \quad (3)$$
$$V_{CLc} = \frac{(V_{Sc} + (Z_{Lc}/Z_{NCb}) * V_{ESC})}{(1 + Z_{Lc}/Z_{NCc} + Z_{Lc}/Z_{CLc})}$$

Substituting Eq. 3 in Eq. 1 the line currents can be expressed as:

$$\begin{aligned} I_{La} &= V_{Sa}(b_1 + jb_2) + V_{ESa}(b_3 + jb_4) \\ &= (V_{Sa}b_1 + V_{ESA}b_3) + j(V_{Sa}b_2 + V_{ESa}b_4) \\ I_{Lb} &= V_{Sb}(b_5 + jb_6) + V_{ESb}(b_7 + jb_8) \\ &= (V_{Sb}b_5 + V_{ESb}b_7) + j(V_{Sb}b_6 + V_{ESb}b_8) \\ I_{Lc} &= V_{Sc}(b_9 + jb_{10}) + V_{ESc}(b_{11} + jb_{12}) \\ &= (V_{Sc}b_9 + V_{ESc}b_{11}) + j(V_{Sc}b_{10} + V_{ESc}b_{12}) \end{aligned} \quad (4)$$

where,

$$b_1 + jb_2 = \frac{\frac{1}{Z_{NCa}} + \frac{1}{Z_{CLa}}}{1 + \frac{Z_{La}}{Z_{NCa}} + \frac{Z_{La}}{Z_{CLa}}}$$
$$b_3 + jb_4 = \frac{\frac{Z_{La}}{Z_{NCa}}\left(\frac{1}{Z_{NCa}} + \frac{1}{Z_{CLa}}\right)}{1 + \frac{Z_{La}}{Z_{NCa}} + \frac{Z_{La}}{Z_{CLa}}} - \frac{1}{Z_{NCa}} \quad (5)$$

$$b_5 + jb_6 = \frac{\frac{1}{Z_{NCb}} + \frac{1}{Z_{CLb}}}{1 + \frac{Z_{Lb}}{Z_{NCb}} + \frac{Z_{Lb}}{Z_{CLb}}}$$
$$b_7 + jb_8 = \frac{\frac{Z_{Lb}}{Z_{NCb}}\left(\frac{1}{Z_{NCb}} + \frac{1}{Z_{CLb}}\right)}{1 + \frac{Z_{Lb}}{Z_{NCb}} + \frac{Z_{Lb}}{Z_{CLb}}} - \frac{1}{Z_{NCb}} \quad (6)$$

$$b_9 + jb_{10} = \frac{\frac{1}{Z_{NCc}} + \frac{1}{Z_{CLc}}}{1 + \frac{Z_{Lc}}{Z_{NCc}} + \frac{Z_{Lc}}{Z_{CLc}}}$$
$$b_{11} + jb_{12} = \frac{\frac{Z_{Lc}}{Z_{NCc}}\left(\frac{1}{Z_{NCc}} + \frac{1}{Z_{CLc}}\right)}{1 + \frac{Z_{Lc}}{Z_{NCc}} + \frac{Z_{Lc}}{Z_{CLc}}} - \frac{1}{Z_{NCc}} \quad (7)$$

Eq. 4 can be expressed as:

$$\begin{aligned} I_{La} &= I_{da} + jI_{qa} \\ I_{Lb} &= I_{db} + jI_{qb} \\ I_{Lc} &= I_{dc} + jI_{qc} \end{aligned} \quad (8)$$

where, I_{da}, I_{db}, and I_{dc} represent the active components of the fundamental line currents and I_{qa}, I_{qb}, and I_{qc} denote the reactive components. From Eq. 4 and 8, it can be observed that the active and reactive

components of the fundamental line current can be varied by varying the ES output voltage V_{ES}. Finally, the neutral current, I_N, is given by:

$$I_N = I_{LA} + I_{LB} + I_{LC} \tag{9}$$

4. Power quality (PQ) assessment

The PQ is a major concern with unbalanced and non-linear loads connected to a distribution system. This requires a proper assessment of the PQ. The improvement in PQ has been assessed for the proposed system using integral PQF. The PQF comprises the following power quality aspects: current unbalance factor (IUNB), total current harmonic distortion (ITHD), and phase displacement between the fundamental voltage and current using the orthogonal current factor (OCF). The PQF indicator value ranged between 1 and 0. A value close to 1 indicates that the overall PQ of the system is high. The expression for PQF, which relates all the above-mentioned power quality indices [29], has been discussed in the following subsections.

4.1. Total harmonic distortion of current (ITHD)

$$QA_1 = ITHD = {}^{I_{eH-A}}/_{I_{e1}} \tag{10}$$

where, $I_{eH\text{-}A}$ is the equivalent harmonic adjusted current and I_{e1} is the equivalent phase current at the fundamental frequency as defined in IEEE Std. 1459-2010.

$$I_{eH-A}^2 = \sum_{h\neq 1} D_h^2 \left({}^{I_{ah}^2 + I_{bh}^2 + I_{ch}^2}/_3\right) \tag{11}$$

where, D_h is the appropriate weighting factor.

$$I_{e1}^2 = {}^{I_{ah}^2 + I_{bh}^2 + I_{ch}^2}/_3 \tag{12}$$

4.2. Current Unbalance Factor (IUNB)

The increased unbalanced current flowing through the distribution network may cause increased line loss and overloading of the neutral conductor, which can cause deterioration of the PQ value of the system. The IUNB determines the degree of unbalanced current flowing in the system.

The IUNB is given by:

$$QA_2 = IUNB = {}^{[I_{e1}^2 - (I^+)^2]^{\frac{1}{2}}}/_{I_{e1}} \tag{13}$$

where, I^+ denotes the positive sequence element of the fundamental component of the current. The equivalent current I_{e1}, has been determined by applying the symmetrical component method

4.3. Orthogonal Current Factor (OCF)

The classical definition of the power factor for unbalanced and non-sinusoidal conditions has been modified by a factor called OCF. The PQ factor gives the degree of phase shift between the fundamental frequency voltage and current and is given by:

$$QA_3 = OC = \frac{I_{1a}\sin\varphi_{1a} \pm I_{1b}\sin\varphi_{1b} \pm I_{1c}\sin\varphi_{1c}}{I_{1a}+I_{1b}+I_{1c}} \quad (14)$$

where, I_{1a}, I_{1b}, and I_{1c} denote the RMS values of the currents in the three phases, φ_{1a}, φ_{1b}, and φ_{1c} represent the phase angle differences between the phase voltage and current at the fundamental frequency.

4.4. PQ evaluation using PQF

The gross PQ of the distribution system with unbalanced loads has been assessed using PQF. The weighted sum of the PQ aspects (ITHD, IUNB, and OCF) determines PQF [29].

$$PQF = \sum_k w_k(1 - QA_k) \quad (15)$$

Here, w_k denotes the weight of the PQ aspects considered. For the study IUNB of 0.35, current THD of 0.3, and OCF of 0.35 represent the values of w_k considered. QA_k indicates the parameters of the power quality for k =1, 2, 3, etc., as introduced in Eq. (10), (13), and (14).

5. Optimised controller of ES

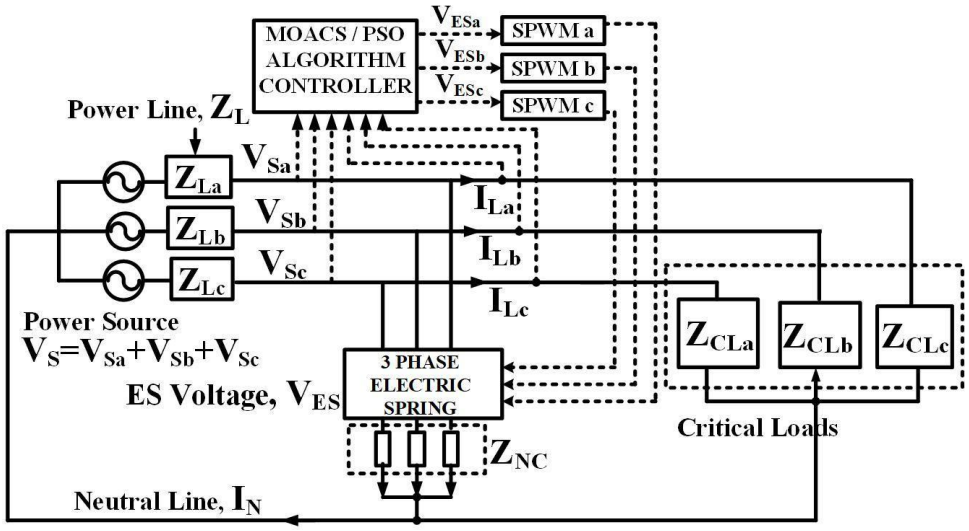

Fig. 4 Block diagram of the proposed ES scheme showing controller action

The design of an appropriate controller for the operation of an ES to maintain the required active and reactive power flow is essential. Based on the mode of operation of ES, an input current controller has been developed to regulate the line current. A block diagram of the ES with current controller coupled to the distribution network is depicted in Fig. 4. A controller based on the MOACS algorithm computes the optimized reference voltage for the ES. Line current I_L and voltage V_S have been decomposed into active (direct axis) and reactive (quadrature axis) components. The controller provides the reference voltages V_{ESa}, V_{ESb}, and V_{Esc}, which are fed to the ES through sinusoidal pulse width modulation (SPWM) generators. A phase-locked loop (PLL) block has been integrated to synchronize all collected variables under a fixed fundamental frequency of 50 Hz. The fundamental system frequency has been generated by the PLL, which provides a reference vector with a phase angle of 0°. Upon receiving SPWM signals, the inverter legs operate independently as half-bridge inverters. The harmonic mitigation block in the controller acquires the harmonic components in the line current through a fast Fourier transformation. The reference harmonic current magnitudes have been set to zero, and the harmonic components of the current have been fed back to the proportional controller. The controller processes the harmonic component magnitude errors and generates ES reference voltages for the harmonic orders.

5.1 Multi objective artificial cooperative search (MOACS) optimization technique

An optimization technique has been implemented to minimize the neutral current and enhance the power factor of the network connected to different types of loads. Earlier studies used single-objective optimization methods such as GA [17] and PSO [18], in which only one objective function could be optimized. The authors in the present study aim to optimize two objective functions as mentioned above through the proposed scheme. Hence, the MOACS algorithm has been employed as an optimization technique [21].

In MOACS, for f_1, f_2, and f_x objective functions, the optimization problem can be formulated as:

$$\text{minimise } \{f_{1(t)}, f_{2(t)}, \text{----} f_{x(t)}\} \tag{16}$$

where, x and t represent the total numbers of objective functions and decision vectors restricted to the workable search space. Multiple objectives result in multiple solutions of a non-dominating nature (a set of

such non-dominating solutions specified as Pareto front) that can be collected using an appropriate algorithm. Thus, the powerful MOACS algorithm is useful for minimizing the two objective functions and helps to improve the PQ of the ES-integrated distribution system. The algorithm is the modification of the artificial cooperative search (ACS) algorithm. The ACS algorithm is a meta-heuristic global search algorithm motivated by different species of nature or superorganisms (e.g., butterflies). These superorganisms move in search of food, interact with one another, and ultimately find the best solution. The MOACS algorithm similarly solves multi-objective issues by employing non-dominated sorting and the principle of crowding distance. Initially the objective function is defined and the population is initialized [21] as:

Minimise $f(T)$ (17)

subjected to $Ti_{LOW} \leq Ti \geq Ti_{UP}$ (i = 1,2,…Q).

Next, the two super-organisms are initialized randomly subject to the boundary limits as follows:

$$\begin{aligned} A_{(i,j)} &= LOW_j + rnd.(UP_j - LOW_j) \\ B_{(i,j)} &= LOW_j + rnd.(UP_j - LOW_j) \end{aligned} \quad (18)$$

where, i= *1*----N, N is the size of the population, j= *1*--- Q, and Q is the problem dimension. For every sub-organism of (A, B), the fitness value ($f(T)$…) is assessed. The objective function is given by:

Minimise $f(t) = \sum_{i=1}^{n} W_i * f_i'(t)$ (19)

where, W_i is the weighted coefficient considered as 0.5, and n denotes the number of objective functions which has been set as two in this study. In this study, the objective functions f_1' and f_2' can be expressed as:

$$\begin{aligned} f_1' &= a + b + c \\ where\ \ & \begin{aligned} a &= 1 - pf_a \\ b &= 1 - pf_b \\ c &= 1 - pf_c \end{aligned} \\ \{f_2' &= abs(I_{na} + I_{nb} + I_{nc})\} \end{aligned} \quad (20)$$

The constraint is,

$$\text{if } \begin{aligned} pf_a < 0.95; a &= pf_a + penalty \\ pf_b < 0.95; b &= pf_b + penalty \\ pf_c < 0.95; c &= pf_c + penalty \end{aligned}$$

$f_1'$is the first objective function to maximize the power factor. Here, pf_a, pf_b, *and* pf_c represent the power factor of the three phases. f_2' is the second objective function to minimize the neutral current. A suitable penalty must be added if the power factor is less than 0.95. The MOACS algorithm has been executed with 200 iterations, and the final non-dominated Pareto-front solution has been saved as the output. Compared to single objective optimization, determining the quality of multi-objective optimization solutions is more difficult. An effective multi-objective optimization algorithm should produce rank one solutions that are closer to the ideal genuine Pareto front and the non-dominated Pareto front solutions should be evenly distributed with less distance between them, and.

Fig. 5 shows the Pareto-front solution output. The graph will be a true optimal Pareto-front if it achieves a rank 1 solution and the solution obtained is uniformly disbursed with a minimum spacing. The figure shows uniform distribution of the solution with minimum and equal spacing. Here, functions 1 and 2 represent the power factor and the neutral current, respectively. It can be observed that function 1, which is the power factor, reaches near the optimal value of 1, and function 2, which represents neutral current, also reaches near the optimal value of 0. The flow chart of the algorithm is shown in Fig. 6 which explains the steps to obtain the global best solution.

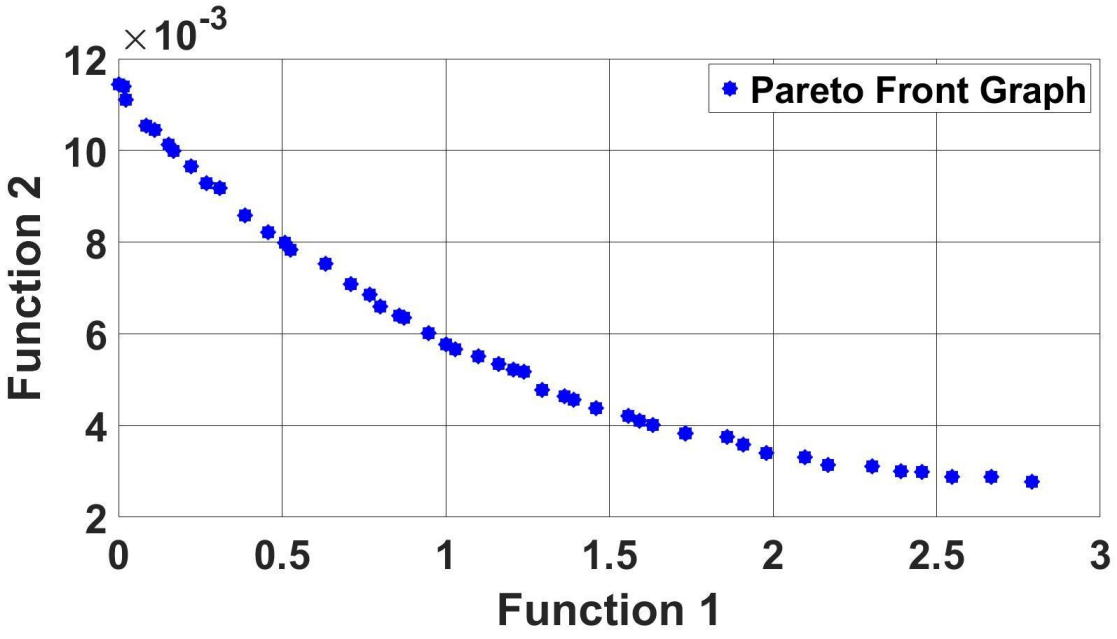

Fig. 5 Optimal Pareto front from MOACS algorithm

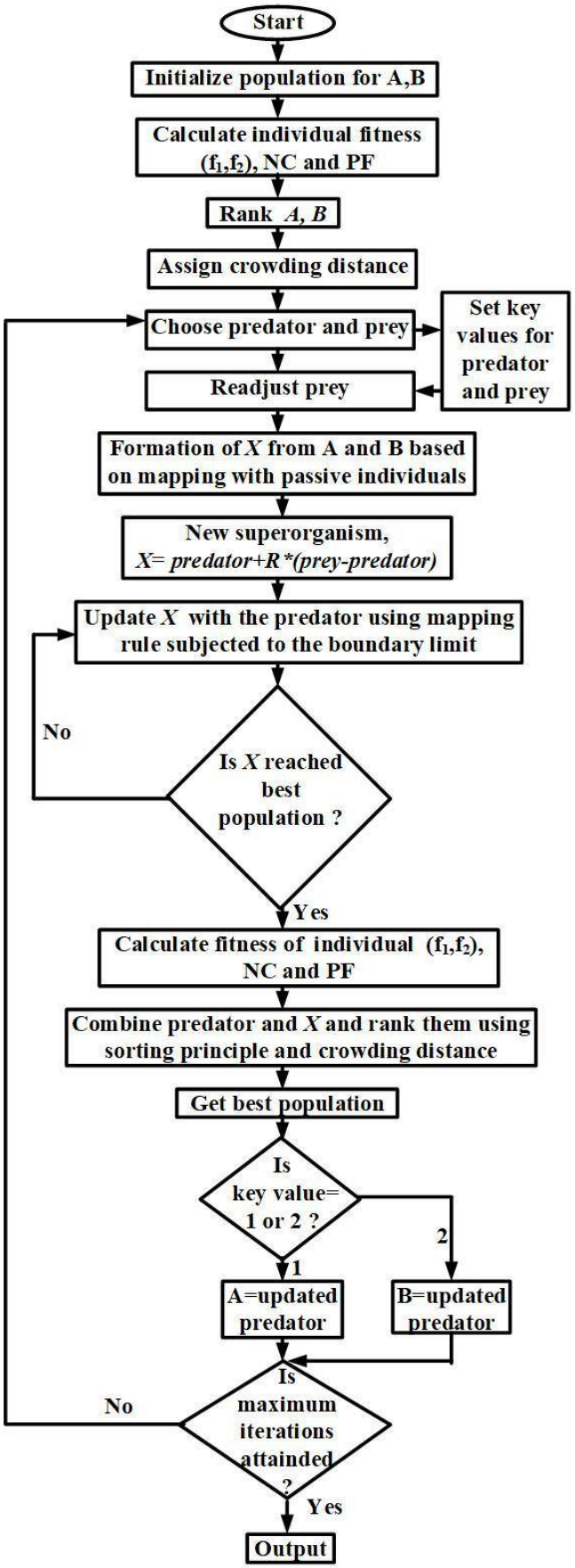

Fig. 6 Flowchart of the MOACS algorithm

6. Simulation results

A simulation study has been conducted on a distribution system with and without an ES connected to the system with various types of loads and during sudden load changes. Power quality parameters, such as the power factor, neutral current, and harmonics, have been monitored to assess the MOACS-based optimized controller operation. The voltage regulation has been computed by measuring the critical load voltage V_{CL} for the loads considered, which indicates the efficiency of the developed scheme. A study has also been conducted considering the presence of intermittent sources in the system.

6.1 Case study I -under unbalanced load

Six different critical resistive-inductive loads have been considered in this investigation. Table 1 demonstrates that the power factor improves to 1 or becomes nearly equal to 1 when ES is turned on. In addition, the neutral current is minimized with the implementation of ES. Table 2 presents the results for the voltages across Z_{CL}. When the ES is connected, the voltage across the CL is regulated and is close to the reference voltage V_{ref} of *200* V. It can be observed that for all loads considered, the voltage regulation is within 3%, which confirms the reliability of the proposed system. Fig. 7(a) shows the power factor improvement with unbalanced loads of *10+j16* Ω, *15+j20* Ω, and *16+j22* Ω in Table 1 connected to the system. The figure shows that a power factor of 0.86 and below without compensation improves to near unity when the ES is connected at 0.5 s, which acts as a reactive power compensator. Fig. 7(b) shows the neutral current for the same set of unbalanced loads. As shown in the figure, the neutral current of 5.076 A obtained without ES connected to the system gets reduced to 0.0175 A after the connection of ES. The voltage fluctuation of the CL before and after the connection of the ES can be observed in Fig. 7(c). The voltage has been regulated to the same levels in three phases following the ES connection. The voltage waveform across the NCL is shown in Figure 7(d). V_{NC} remains the same for all three phases before 0.5 s, as can be observed from the figure. Soon after the ES turns on, the voltage across the NCL gets modulated, and this combination works together as an SL to enhance system PQ. The PQ of the system as assessed by different power quality factors has been specified in Table 3. The power quality factors (IUNB, OCF, and ITHD) have been taken into account when computing the PQF, both with ES connected and disconnected.

The result shows that the PQF with ES connected attains a value above 0.9 for all considered loads. This indicates an improved PQ with the implementation of the optimized ES.

Table 1. Results for power factor and neutral current without and with ES

Critical Load Impedance			ES	Power Factor			I_N (A)
a	b	c		a	b	c	
12+j17	9+j15	13+j16	Without	0.8508	0.9060	0.8926	5.0168
			With	0.9900	1.0000	1.0000	0.0190
10+j16	9+j20	11+j19	Without	0.8554	0.8795	0.8668	5.0390
			With	0.9800	0.9900	0.9900	0.0243
11+j20	8+j18	10+j22	Without	0.8358	0.8721	0.8800	4.7690
			With	0.9800	0.9900	0.9890	0.0326
10+j18	j20	12+j23	Without	0.8794	0.7071	0.8981	4.9980
			With	0.9800	0.9554	0.9900	0.0330
10+j16	15+j20	16+j22	Without	0.8546	0.8668	0.8420	5.0760
			With	1.0000	0.9865	0.9925	0.0175
13+j22	15+j30	18+j17	Without	0.9100	0.8800	0.9144	4.8966
			With	1.0000	0.9900	1.0000	0.0120

Table 2. Results for voltage regulation without and with ES

Critical Load Impedance (Ω)			ES	Critical Load Voltage (V)			Voltage Regulation (%)		
a	b	c		a	b	c	a	b	c
12+j17	9+j15	13+j16	Without	189.3	188.5	189.3	5.65	6.1	5.65
			With	198.2	197.8	198.2	0.98	1.11	0.98
10+j16	9+j20	11+j19	Without	189.9	190.7	191.0	5.31	4.87	4.71
			With	199.6	198.2	198.5	1.21	1.01	0.75
11+j20	8+j18	10+j22	Without	190.2	189.1	190.5	5.15	5.76	4.98
			With	199.7	199.1	198.7	0.65	0.95	0.65
10+j18	j20	12+j23	Without	190.5	186.1	189.2	4.98	5.26	4.93
			With	199.0	198.9	199.3	0.50	0.60	0.50
10+j16	15+j20	16+j22	Without	188.0	190.8	185.8	5.82	4.82	4.82
			With	199.4	199.8	199.2	1.01	0.60	0.40
13+j22	15+j30	18+j17	Without	191.0	191.5	191.3	4.71	4.43	4.54
			With	198.2	199.4	198.8	0.98	0.30	0.60

Table 3. Results of PQ factors (PQF)

Critical Load Impedance (Ω)			ES	IUNB	OCF	PQF
a	b	c				
12+j17	9+j15	13+j16	Without	0.6537	0.4659	0.6084
			With	0.1147	0.0214	0.9516
10+j16	9+j20	11+j19	Without	0.2251	0.5263	0.7379
			With	0.0986	0.0512	0.9468
11+j20	8+j18	10+j22	Without	0.1978	0.3986	0.7912
			With	0.1203	0.0365	0.9153
10+j18	j20	12+j23	Without	0.5467	0.4895	0.6373
			With	0.0363	0.0258	0.9773
10+j16	15+j20	16+j22	Without	0.8935	0.4360	0.5241
			With	0.1052	0.0374	0.9403
13+j22	15+j30	18+j17	Without	0.8100	0.4749	0.4837
			With	0.1241	0.0000	0.9572

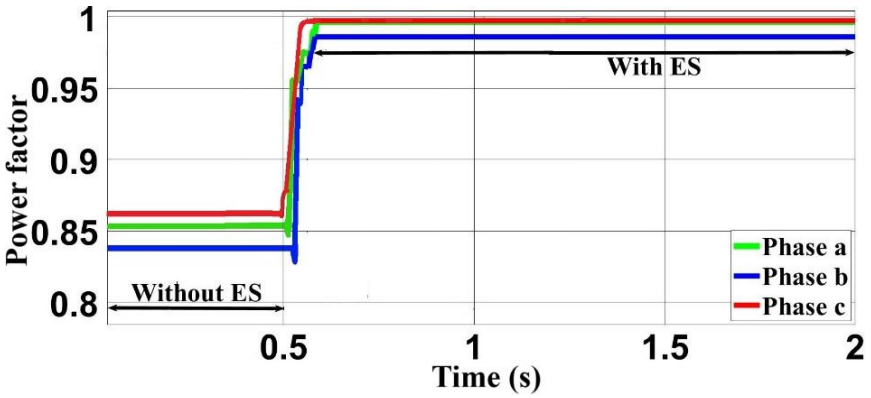

(a)

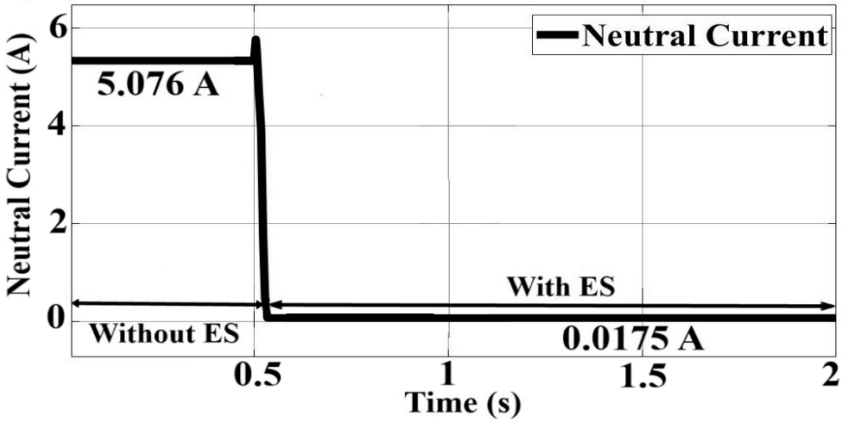

(b)

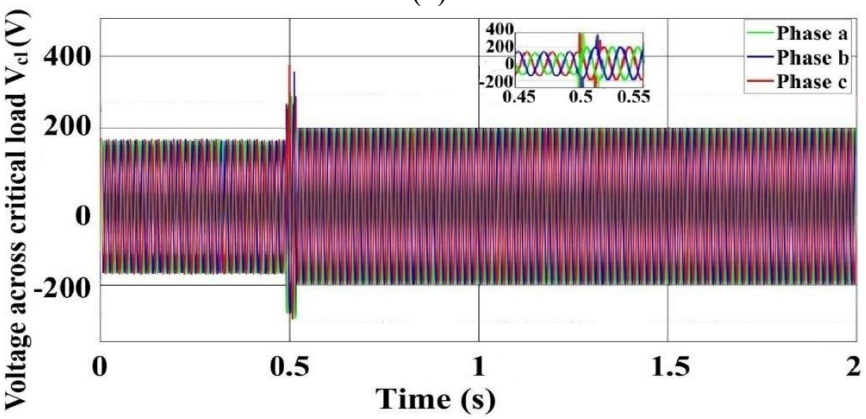

(c)

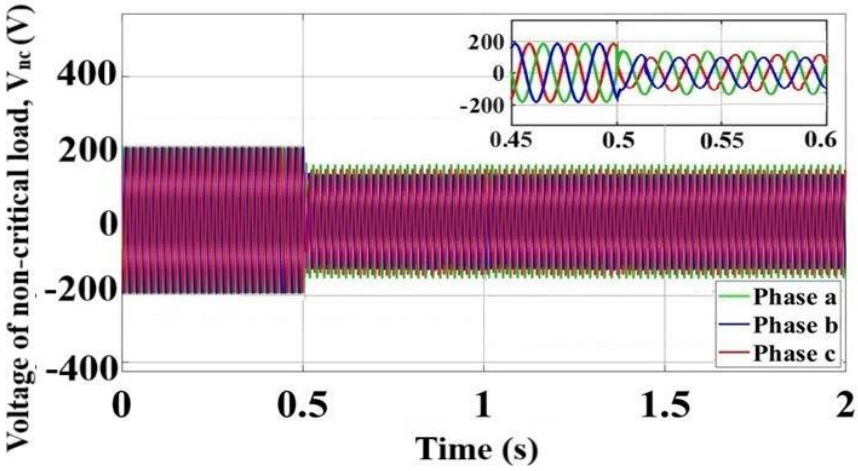

(d)

Fig. 7 Performance of ES under unbalanced load (a) Power factor improvement (b) Neutral current reduction (c) CL voltage & (d) NCL voltage.

6.2 Case study II- under sudden load change

The proficiency of the ES compensator has been verified under sudden load variations. For the loads *10+j16 Ω*, *15+j20 Ω*, and *16+j22 Ω* in phases 'a', 'b', and 'c' respectively, the load in phase 'c' is changed suddenly at t = 0.5 s from *16+j22 Ω* to *14+j24 Ω*. The ES acts immediately to regulate the voltage across the CL. Fig. 8(a) shows that from t = 0 s to 0.5 s, the voltage waveform has been well regulated and balanced by ES. At t = 0.5 s, as the load changes suddenly, the ES voltage also changes, as shown in Fig. 8(b), and regulates the CL voltage. Fig. 8(c) shows the variation in the power factor with an abrupt load change. It can be observed that the power factor changes from 0.9865 to 0.9961 in phase 'b'; from 0.9925 to 0.9810 in phase 'c'; and remains unchanged for phase 'a'.

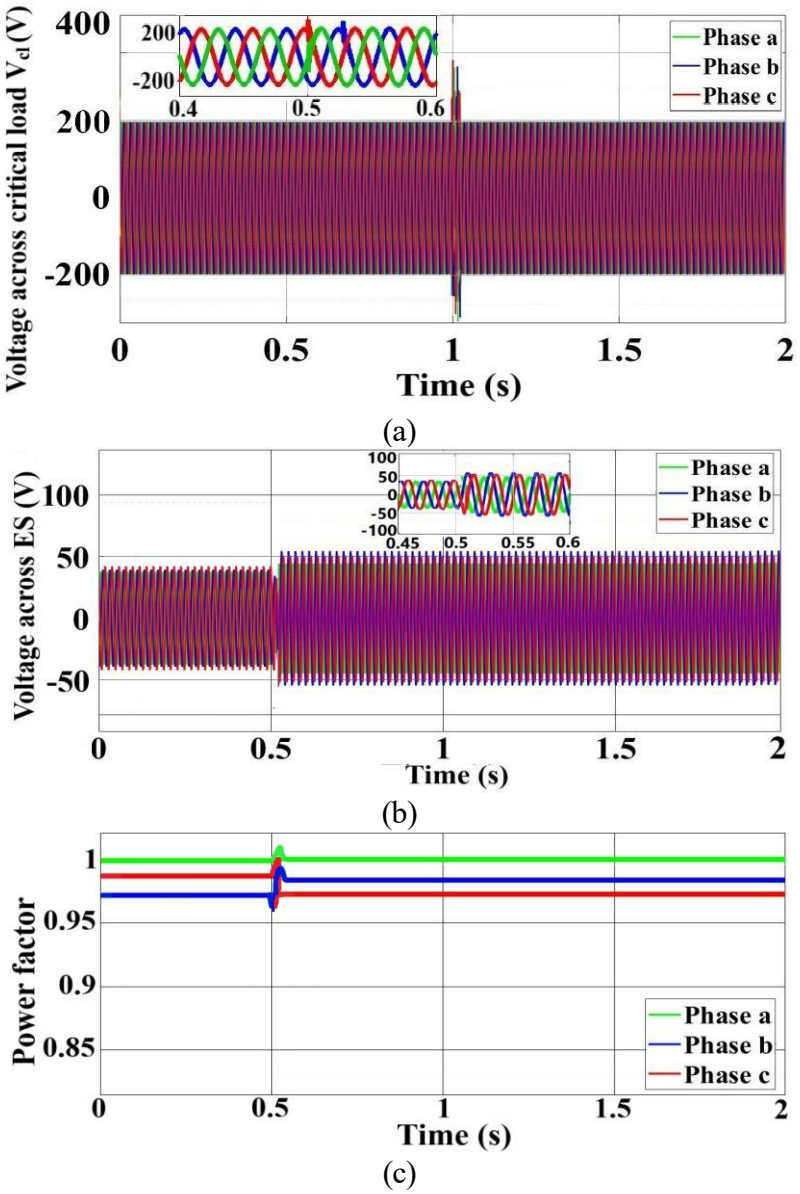

Fig. 8 Performance of the ES under sudden change of load (a) Voltage waveform of the critical load (b) Voltage waveform of ES and (c) Power factor

6.3 Case study III- with intermittent energy source

One of the issues that a low-voltage distribution system faces with the connection of an intermittent energy source (IES) is the variation in the source-end voltage. To study the system under this condition, a controlled current source, representing an IES, has been incorporated into the system, the diagram of which is shown in Fig. 9(a). The controlled current source, i.e., IES, injects peak current (I_P) of 0 A, 2 A, and 8 A peak amplitude and then steps down to 3 A, as shown in Fig. 9(b). The durations of the steps are 2 s and 4 s. The variation in the system voltage is shown in Fig. 9(c). Throughout the operation, the CL voltage has been regulated by the ES at 200 V. The MOACS-optimized SL controller generates the reference voltage for the ES in every step, as shown in Fig. 9(d), and the ES in turn operates either in the inductive or capacitive mode to regulate the system voltage.

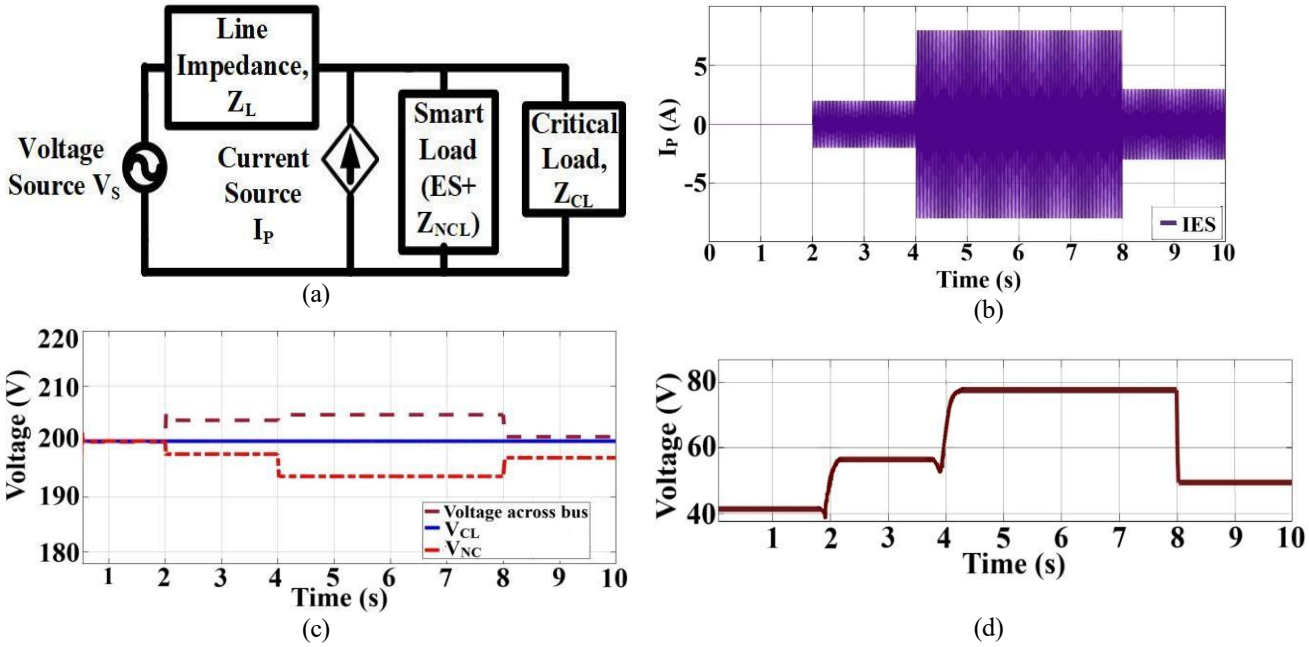

Fig. 9 Performance of ES connected to intermittent energy source (a) Schematic diagram (b) Current waveform (c) Voltage waveforms of bus voltage, critical load and non-critical load and (d) Voltage waveform of ES

The study has been further carried out to observe the impact of IES injection on the system for a time period of 15 s in every step. The total duration has been considered as 60 s for this study. The variation in peak current (I_P), by the IES is shown in Fig. 10(a). When IES injects 2 A into the system, the voltage rises to 208.5 V. After that, when IES injects 8 A, bus voltage rises to 216 V and further to 218 V at the end of the 15 s duration. The increase in voltage is 8 V compared to 5 V when the IES remains connected

for 2 s. In the last step, when IES injects 3A for 15 s, the bus voltage falls to 201.5 V. Hence, there is a rise of 2.5 V compared to 0.5 V in the previous case. However, with the connection of ES to the system, the critical load voltage fluctuation has been arrested. The variation in bus voltage, non-critical load voltage (V_{NC}) and critical load voltage (V_{CL}) can be observed in Fig. 10(b). ES operates in capacitive mode when the bus voltage falls below the nominal value. On the contrary, when the bus voltage rises, the ES connected to the system operates in the inductive mode. It can be further observed that the critical load voltage (V_{CL}) throughout the duration has been strictly maintained at 200 V. Fig. 10(c) shows the variation of voltage across ES.

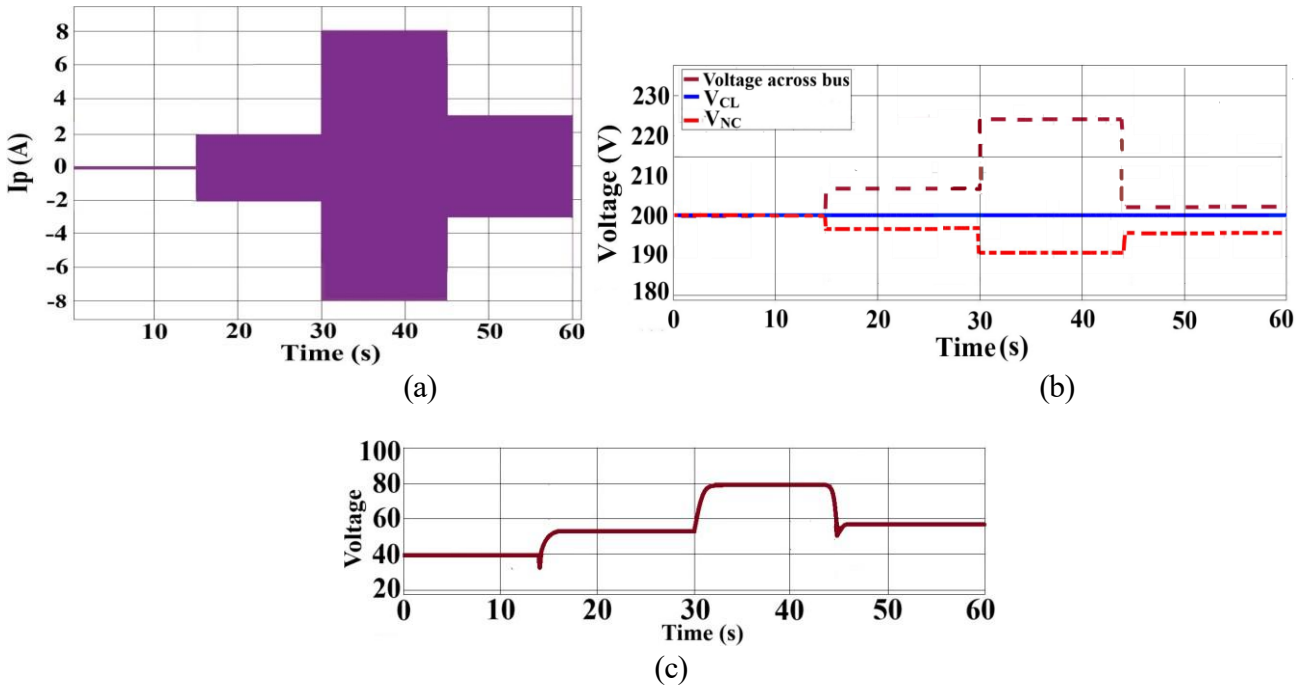

Fig. 10 Responses of step changing IES injection for longer duration showing a) controlled IES current b) voltage across critical, non-critical load and bus voltage and c) ES voltage.

6.4 Case study IV- with real time digital simulator

The real-time simulator OPAL-RT has been utilized to verify the simulation findings that were achieved using Matlab Simulink. To enable the digital simulator to solve the model equations, the simulation model has been set up to execute in discrete time steps. To run the OPAL-RT software, the simulator and the prepared software model have been synchronized. In order for the simulator to validate the simulation findings, the time step duration has been set to correspond with the system frequency response. Fig. 11(a), (b), and (c) show the neutral current, critical load voltage, and power factor, respectively. Unbalanced loads of *10+j16 Ω*, *9+j20 Ω,* and *11+j19 Ω*, have been considered. Fig. 11(a), shows that the neutral current of 5

A flowing through the system before the connection of ES at 0.5 s gets reduced to 0.05 A with ES. As shown in Fig. 11(b), the critical load voltage remains unbalanced and below the reference voltage level before the ES gets turned on. After the triggering of the ES at 0.5 s, the unbalance decreases and the voltage regulation improves to 0.53%. Fig. 11(c) shows that with the activation of ES at 0.5 s, the power factor also improves from 0.9 to nearly 0.98.

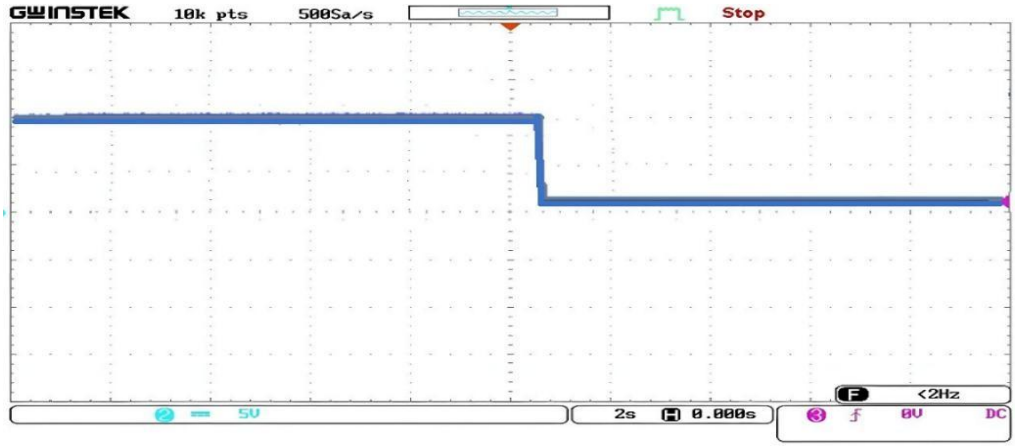

(a)

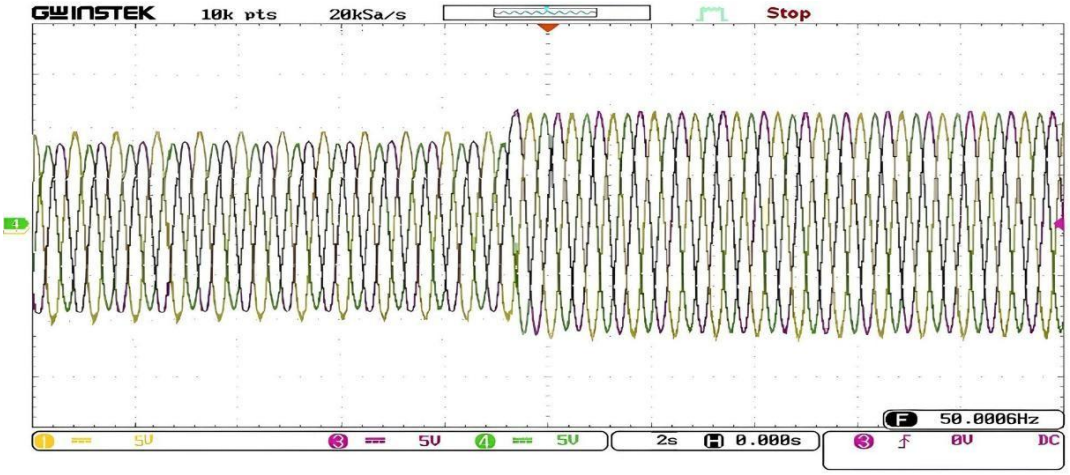

(b)

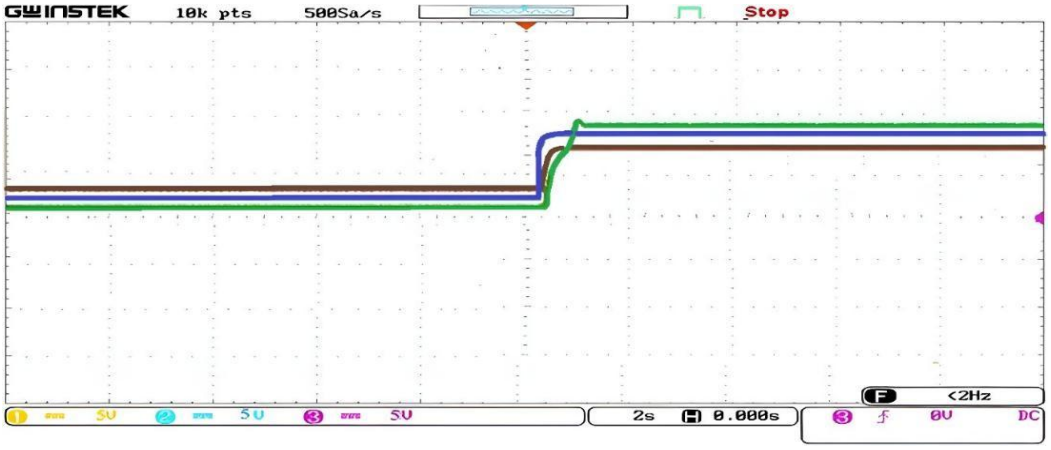

(c)

Fig. 11 Real time simulation waveform of (a) Neutral current (b) Critical load voltage (c) Power factor

7. Comparative Analysis

7.1 Comparison of proposed MOACS optimised ES with PSO optimised ES

The results acquired using the MOACS algorithm have been compared with those of the PSO algorithm for the optimized operation of the ES. Both the algorithms have been executed for 200 iterations. The outcome of each algorithm is fed to the ES to generate voltage V_{ES} for the loads listed in Table 4. The generated V_{ES} accordingly modulates the line current, and the results obtained for the power factor and neutral currents are tabulated. Compared to the PSO-based controller, the MOACS-based controller produces better outcomes.

Table 4. Results of PSO, HS, and MOACS algorithm

Critical Load Impedance			ES	Power Factor			I_N (A)
a	b	c		a	b	c	
12+j17	9+ j15	13+j16	Without	0.8508	0.9060	0.8926	3.368
			With PSO	0.9643	0.9899	0.9810	1.7813
			With HS	0.9847	0.9800	0.9200	0.2721
			With MOACS	0.9900	1.000	1.000	0.0190
10+j16	9+ j20	11+ j19	Without	0.8554	0.8795	0.8668	1.4090
			With PSO	0.9671	0.9804	0.9912	0.0904
			With HS	1.0000	0.9807	0.9833	0.0367
			With MOACS	0.9800	0.9900	0.9900	0.0243
11+j20	8+ j18	10+j22	Without	0.8358	0.8721	0.8800	1.3690
			With PSO	0.9678	0.9815	0.9853	0.2940
			With HS	0.9000	0.9535	0.9890	0.5094
			With MOACS	0.9800	0.9900	0.9890	0.0326

7.2 Comparison of proposed MOACS optimised ES with HS optimised ES

To validate the optimality of the system, another optimization technique known as harmony search (HS) optimization has been applied. The algorithm produced optimized results after executing it for 10000 iterations compared to 200 iterations in MOACS. Table 4 shows the results obtained from the HS technique also. The outcome of the HS technique shows that neutral current (I_N) for all the loads is more than the optimum neutral current obtained with the MOACS algorithm. The HS technique shows an inferior power factor in all phases for loads 1 and 3 compared to MOACS optimized outputs. The overall results highlight that MOACS performs better than the HS technique optimizing both the objective functions. Separate

pareto diagrams have been obtained while implementing the HS algorithm for the two objective functions working separately as well as in combination. Fig. 12(a) shows the Pareto diagram when only power factor has been considered as the objective function and Fig. 12(b) depicts the same when only neutral current has been considered as the objective function. In Fig. 12(c), both power factor and neutral current have been incorporated in the objective function. The rseults of PQF obtained with PSO, HS and MOACS are depicted in Table 5.

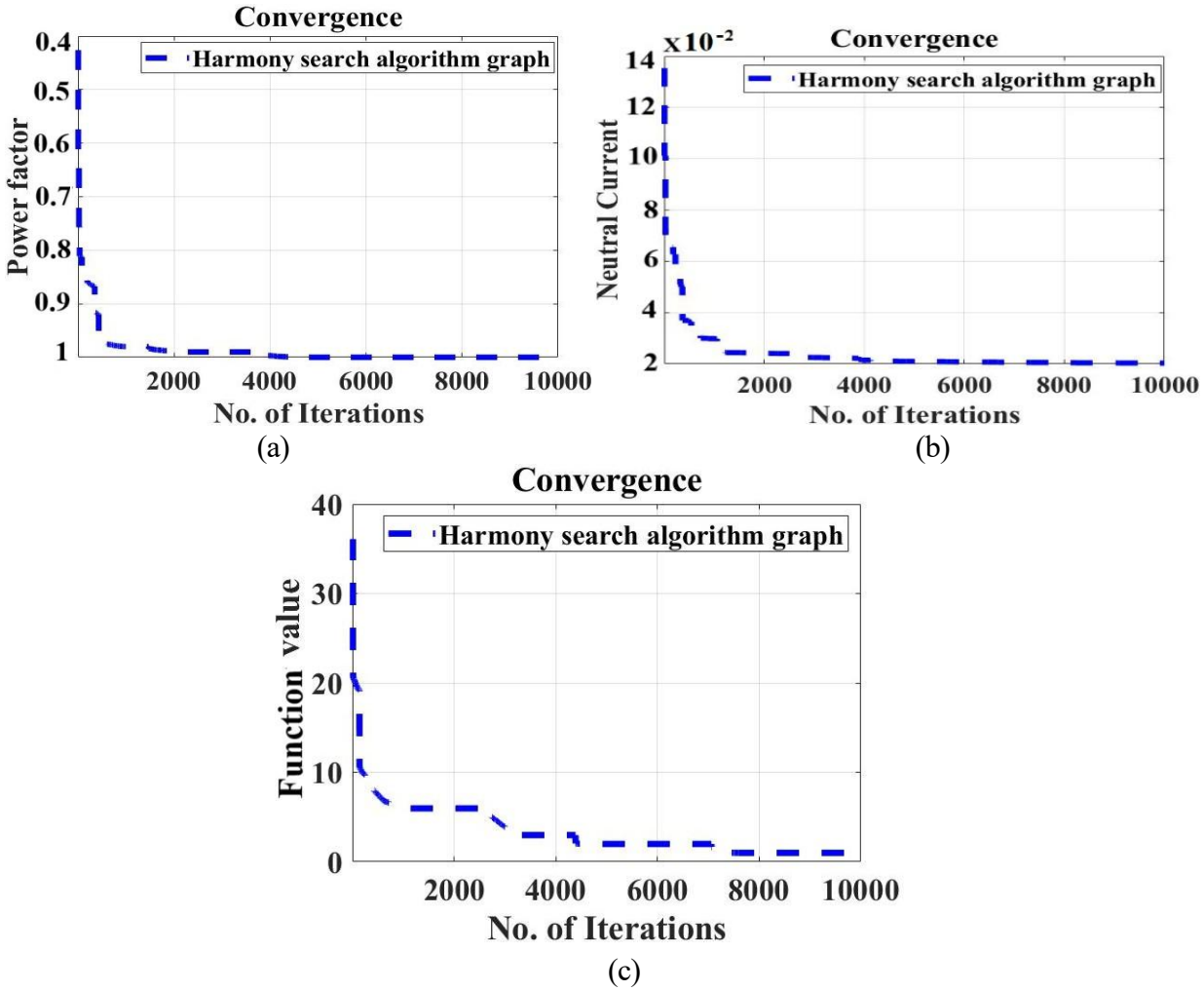

Fig. 12 Optimal solution obtained by HS algorithm for (a) Power factor as objective function (b) Neutral current as objective function and (c) Combined objective functions

Table 5. Comparative assessment of PQF

Critical Load Impedance			PQF		
a	b	c	With PSO	With HS	With MOACS
12+j17	9+ j15	13+j16	0.9136	0.9072	0.9465
10+j16	9+ j20	11+ j19	0.9257	0.9324	0.9392
11+j20	8+ j18	10+j22	0.9146	0.8985	0.9307

7.3 Comparison of proposed scheme with other compensator schemes

The ES as a reactive power compensator has been compared to other compensator schemes. For the balanced load, as shown in Table 6, a comparison is made in terms of the THD of the source current and the average reactive power, Qs, extracted from the source. In comparison to other compensators, the ES compensator gives the lowest THD. A comparative study has also been carried out considering unbalanced loads to show better power factor improvement in comparison to the compensator scheme used in [25, 50, and 531], and the results are presented in Table 7.

Table 8 shows the structured comparison of different controlling methodologies of ES along with its features. It can be observed that the ES feature proposed in [4] is capable of regulating voltage and provides damping for maintaining grid stability. Control methods proposed in [6, 19] can also improve power factor apart from voltage support. Controllers proposed in [9] and [18] are capable of minimizing harmonics apart from voltage support and power factor improvement. Controllers used in [17, 20] show that proficiency of ES in unbalance minimization other than voltage regulation and power factor improvement, respectively. However, the proposed MOACS controller shows efficient performance for all the ES features mentioned above.

Table 6. Comparative assessment of average reactive power and total harmonic distortion

Load (KVA)			Past and present studies	Avg. Q_s (KVAr)	THD (%)
a	b	c			
25+j25	25+j25	25+j25	Kulkarni D B et al [50]	4.55	11.53
			Das S et al [51]	1.60	1.14
			Dey S et al. [25]	2.70	0.98
			Present work	1.67	0.24

Table 7. Comparative assessment of power factor

Load (KVA)			Studies	Power Factor		
a	b	c		a	b	c
2+j1	3+j1.5	4+j2	Without	0.8940	0.8940	0.8926
			Das S et al.	0.9680	0.9870	0.9680
			Present work	0.9841	0.9910	0.9850
15+j22	17+j26	17+j24	Without	0.5500	0.5300	0.5700
			Dey S et al.	0.9500	0.9600	0.9600
			Present work	0.9820	0.9833	0.9833
14+j26	13+j20	16+j26	Without	0.4700	0.5400	0.5200
			Dey S et al.	0.9700	0.9600	0.9700
			Present work	0.9927	0.9900	0.9927

Table 8. Performance comparison between different control methodologies

Referred studies	ES features				Controller/ Optimization Technique
	Voltage Regulation	Power Factor Improvement	Unbalance Minimization	Harmonic Minimization	
[4]	✓				Pulse width modulation controller
[6]	✓	✓			Generalized controller
[9]	✓			✓	Hysteresis band current controller (HBCC)
[17]	✓		✓		Genetic Algorithm (GA) based controller
[18]	✓	✓		✓	Particle swarm optimization controller
[19]	✓	✓			Rolling-optimization based controller
[20]		✓	✓		Multi-objective continuous genetic algorithm-based controller
Proposed Method	✓	✓	✓	✓	MOACS optimized controller

8. Discussions

When there are more than one objective function and the objective functions are conflicting with each other, it is difficult to obtain a unique optimal solution. Hence, suitable algorithm needs to be implemented to obtain multiple non-dominated solutions. The two objective functions considered in the study are maximization of power factor and minimization of neutral current, which are conflicting in nature. MOACS is based on artificial cooperative search algorithm that can efficiently handle single-objective optimization problems. MOACS is a powerful algorithm to solve multi-objective optimization problems. The performance of MOACS is satisfactory and better than some other multi-objective optimization algorithms [21, 22]. In the present study, performance of MOACS has been compared with two other algorithms, and the obtained results confirm the efficacy of the MOACS.

It has been observed from the simulation results that the reduction of neutral current is more with the MOACS algorithm compared to PSO and HS algorithm. For three different sets of unbalanced loads, the neutral current reduces to 1.78 A, 0.09 A, and 0.29 A from 3.368 A with PSO whereas these values are 0.27 A, 0.036 A, and 0.0509 A respectively with HS. The minimum value of neutral current has been obtained

with MOACS, which are 0.019 A, 0.024 A, and 0.32 A respectively. MOACS also results in maximum improvement of power factor in all ~~the~~ three phases compared to the PSO and HS algorithms. The power quality factors with MOACS are 0.9465,0.9392, and 0.9307 compared to 0.9136, 0.9257, 0.9146 with PSO and 0.9072, 0.9324, 0.8985 with the HS algorithm. Thus, the overall improvement in power quality factor is maximum with MOACS.

The authors in this work have not considered the operational voltage range of the non-critical load. In order to maintain critical load voltage at its nominal value, the non-critical load may experience severe voltage fluctuations. This may be detrimental for the non-critical loads, and no protection strategy for this has been addressed in this paper. When multiple ES operate in a system, fair electricity consumption in each non-critical load should be guaranteed. Along with enhancing voltage stability at each node, consistent output reactive power of all ES and voltage deviation ratio of all non-critical loads should be maintained. The interaction and consensus operation of multiple ESs in a distribution network to cater specific requirements at different locations will be studied in the future. The optimized operation of ES using MOACS in inverter-interfaced microgrids may also be investigated in the future.

9. Conclusion

In this paper an intrinsic assessment of power quality transfer in a distribution network has been carried out through multi-objective optimized operation of ES. The operation of ES has been controlled by the MOACS algorithm, which results in minimizing the unbalance in the system with improved power factor. MOACS algorithm sets the compensation reference and sends to the controller. The effectiveness of the scheme is verified under abrupt changes in load and non-linear loads. The voltage across the critical load has been maintained constant for the change in load and in the presence of intermittent renewable energy source. The performance of MOACS has been compared with PSO and harmony search optimization techniques. It has been established that the MOACS algorithm results in better overall power quality improvement in the system through the assessment of power quality factor. The significant improvement in voltage regulation and power quality with the implementation of the MOACS-based optimized ES has established the potency of this technique.

References

1. Palensky P and Dietrich D 2011 Demand side management: Demand response, intelligent energy systems, and smart loads. *IEEE Transactions on Industrial Informatics*.7(3) 381–388.

2. Wen L, Zhou K, Feng W and Yang S 2024 Demand Side Management in Smart Grid: A Dynamic-Price-Based Demand Response Model. *IEEE Transactions on Engineering Management.* 71 1439-145.

3. Srivastava A K, Kumar A A and Schulz N N 2012 Impact of distributed generations with energy storage devices on the electric grid. *IEEE Systems Journal*. 6(1) 110–117.

4. Hui S Y R, Lee C K and Wu F F 2012 Electric springs—A new smart grid technology. *IEEE Transactions on Smart Grid*. 3(3)1552–1561.

5. Lee C K, Liu H, Tan S C, Chaudhuri B and Hui S Y R 2021 Electric Spring and smart load: technology, system-level impact, and opportunities. *IEEE Journal of Emerging and Selected Topics in Power Electronics*.9(6) 6524–6544.

6. Chen T, Liu H, Lee C K and Hui S Y R 2020 A generalized controller for electric-spring-based smart load with both active and reactive power compensation. *IEEE Journal of Emerging and Selected Topics in Power Electronics*. 8(2)1454–1465.

7. Soni J, Sen B, Kanakesh V K, Panda S K 2018 Performance analysis and evaluation of reactive power compensating electric spring with linear loads. *International Journal of Electrical Power & Energy Systems*.101 116–126.

8. Wang Q, Cheng M, Jiang Y 2016 Harmonics suppression for critical loads using electric springs with current-source inverters. *IEEE Journal of Emerging and Selected Topics in Power Electronics*.4(4)1362–1369.

9. Panda D, Kundu P and Rajpurohit B S 2024 Real-Time Voltage Control and Harmonics Elimination of Islanded Microgrid Using Back-to-Back Electric Spring. *IEEE Transactions on Industry Applications*.; 60(4) 5825-5839.

10. Liu H, Wang M, Li J, Xu X, Xu Z and Dou J 2022 Collaborative control framework of multiple electric springs for frequency stabilization and distribution loss reduction in microgrids. *IEEE Transactions on Smart Grid*. 13(5) 4102–4112.

11. Chen T, Zheng Y, Chaudhuri B and Hui S Y R 2020 Distributed electric spring based smart thermal loads for overvoltage prevention in LV distributed network using dynamic consensus approach. *IEEE Transactions on Sustainable Energy*.11(4) 2098–2108.

12. Yang T, Mok K T, Ho S, Tan S, Lee C and Hui S Y R 2019 Use of integrated photovoltaic-electric spring system as a power balancer in power distribution networks. *IEEE Transactions on Power Electronics*. 34(6) 5312–5324.

13. Liang L, Hou Y, Hill D J and Hui S Y R. Enhancing resilience of microgrids with electric springs 2018 *IEEE Trans. Smart Grid*. 9(3) 2235–47.

14. Wang Q, Ding Z, Cheng M, Deng F and Buja G 2022 Direct power control of three-phase electric springs. *Ind. Electron*. 69(12) 13033–13044.

15. Javaid M S, Sabir A, Abido M A and Bouchekara H R E H 2019 Design and implementation of electric spring for constant power applications. *Electric Power Systems Research.*175.

16. Yan Y, Qin Y, Tan S C and Hui S Y R 2020 Reducing distribution power loss of islanded AC microgrids using distributed electric springs with predictive control. *IEEE Transactions on Industrial Electronics* 67(10) 9001–9011.

17. Yan S, Tan S C, Lee C K, Chaudhuri B, and Hui S Y R 2015 Electric springs for reducing power imbalance in three-phase power systems, *IEEE Trans. Power Electron*. 30(7) 3601–3609.

18. Areed E F, Abido M A, Al-Awami A T and Hussain S A 2020 Electric spring average model development and dynamic analysis for demand-side management. *IET Smart Grid*. 3(2) 226–236.

19. Quijano D A, Feltrin A P and Catalao J P S 2022 Probabilistic rolling-optimization control for coordinating the operation of electric springs in microgrids with renewable distributed generation. *IEEE Transactions on Sustainable Energy* 13(4) 2159–2171.

20. Tinoco G T, Lieberman D G, Rodriguez M V, Cervantes J G A and Perez A G 2022 Modeling of electric springs and their multi-objective voltage control based on continuous genetic algorithm for unbalanced distribution networks. *International Journal of Electrical Power & Energy Systems* 138.

21. Pavankumar Y, Kollu R and Debnath S 2021 Multi-objective optimization of photovoltaic/ wind/biomass/battery-based grid-integrated hybrid renewable energy system. *IET Renewable Power Generation* 15 1528–1541.

22. Pavankumar Y, Debnath S and Paul S 2023 Multi-objective pareto optimal unbalance voltage compensation in the microgrid. *Electric Power Systems Research* 217.

23. Brandao D I, Ferreira W M, Alonso A M S, Tedeschi E and Marafao F P 2020 Optimal multiobjective control of low-voltage ac microgrids: power flow regulation and compensation of reactive power and unbalance. *IEEE Trans. Smart Grid.* 11(2)1239–1252.

24. Naderi Y, Hosseini S H, Zadeh S G, Ivatloo B M, Vasquez J C and Guerrero J M 2018 An overview of power quality enhancement techniques applied to distributed generation in electrical distribution networks. *Renewable and Sustainable Energy Reviews* 93 201-214.

25. De S and Debnath S 2019 Optimal switching strategy of an SVC to improve the power quality in a distribution network. *IET Science, Measurement & Technology* 13(5) 640–649.

26. Luo X, Akhtar Z, Lee C K, Chaudhuri B, Tan S C and Hui S Y R 2015 Distributed voltage control with electric springs: Comparison with STATCOM. *IEEE Trans. Smart Grid* 6(1) 209–219.

27. Savrun M M 2021 Z-source converter integrated dc electric spring for power quality improvement in dc microgrid. *Engineering Science and Technology, an International Journal* 24(6) 1408–1414.

28. Yan S, Tan S C, Lee C K, Chaudhuri B, Hui S Y R 2017 Use of Smart Loads for Power Quality Improvement. *IEEE Journal of Emerging and Selected Topics in Power Electronics* 5(1) 504–512.

29. Sharon D, Montano J C, Lopez A, Castilla M, Borrás D and Gutiérrez J 2008 Power quality factor for networks supplying unbalanced nonlinear loads. *IEEE Transactions on Instrumentation Measurement* 57(6) 1263–1273.

30. Joshi M K and Patel R R 2025 A simulation analysis of reactive power compensation with hybrid compensator in shunt compensated system. *Eng. Res. Express* 7(1) 015328.

31. Kumar A and Choudhary J 2023 Power quality improvement of hybrid renewable energy systems based microgrid for statcom: hybrid-deep-learning model and mexican axoltl dingo optimizer (MADO). *Eng. Res. Express* 5(4) 045031.

32. Munnu M K and Choudhary J 2023 Optimal placement and sizing of custom power devices using APSO and JAYA optimization in radial distribution network. *Eng. Res. Express* 5(1) 015068.

33. Ranjan A and Choudhary J 2023 Enhancement of power quality in grid-connected HRES using UPQC with self-improved Battle Royal Optimizer in IEEE 14 bus system. *Eng. Res. Express* 5(4) 045018.

34. Anbuchandran S, Arumuga B M, Silas S D and Thinakaran M 2024 A hybrid optimization for distributed generation and D-STATCOM placement in radial distribution network: a multi-faceted evaluation. *Eng. Res. Express* 6(3) 035351.

35. Tiwari A and Agarwal R 2022 A comparative analysis of PI & FLC based grid connected PV system with power backup to improve power quality. *Eng. Res. Express* 4(4) 045010.

36. Gandotra R and Pal K 2022 FACTS Technology: A Comprehensive Review on FACTS Optimal Placement and Application in Power System. *Iranian Journal of Electrical and Electronic Engineering* 18(3) 95-109.

37. Shah M S, Ullah M F, Nouman D, Khan M A, Khan T and Waseem M 2024 A review on the state of the art of dynamic voltage restorer: topologies, operational modes, compensation methods, and control algorithms. *Eng. Res. Express* 6(1) 012302.

38. Hilawie A and Shewarega F 2023 Improved multi objective particle swarm optimization based reactive power optimization for ensuring voltage security of power systems. *Eng. Res. Express* 5(4) 045062.

39. Shaikh M S, Raj S, Babu R, Kumar S and Sagrolikar K 2023 A hybrid moth – flame algorithm with particle swarm optimization with application in power transmission and distribution. *Decision Analytics Journal* 6 100182.

40. Shaikh M S, Hua C, Jatoi M A, Ansari M M and Qader A A 2021 Application of grey wolf optimisation algorithm in parameter calculation of overhead transmission line system. *IET Sci. Meas. Technol.* 15 218–231.

41. Shaikh M S, Wang C, Xie S et al. 2025 Coverage and connectivity maximization for wireless sensor networks using improved chaotic grey wolf optimization. *Sci Rep* 15 15706.

42. Wesley B J, Babu G S and Kumar P S 2024 Design and control of LSTM-ANN controllers for an efficient energy management system in a smart grid based on hybrid renewable energy sources. *Eng. Res. Express* 6(1) 015074.

43. Mahdad B 2024 Improved mountain gazelle optimizer based interactive distributed strategy to solving large scale OPF. *Eng. Res. Express* 6(2) 025341.

44. Yin F and Wang C 2025 Consensus control of multiple electric springs considering non-critical load electricity fairness in islanded microgrid. *International Journal of Electrical Power & Energy Systems* 168 110663.

45. Gandotra R and Pal K 2025 EVCS demand management using multi-objective power flow analysis with renewable distributed generators. *Eng. Res. Express* 7(1) 015347.

46. Pal K, Verma K and Gandotra R 2024 Optimal location of FACTS devices with EVCS in power system network using PSO. *e-Prime - Advances in Electrical Engineering* 7 100482.

47. Iqbal S A, Raj S and Shiva C K 2025 A chaotic chimp sine cosine algorithm for optimizing hydrothermal power scheduling. *Chaos, Solitons & Fractals* 192 115972.

48. Ishaq M, Ullah K, Abbass M J and Awais M 2024 Reactive power compensation applications of matrix converter: a systemic review. *Eng. Res. Express* 6(4) 042301.

49. Wang X, Chen X, Huang Z, Zhou M and Zhao C 2025 Research on the working principle and stability of CLC electric springs based on the impedance analysis method. *Int J Circ Theor Appl.* 53(1) 275-290.

50. Kulkarni D B and Udupi G R 2010 ANN-based SVC switching at distribution level for minimal-injected harmonics. *IEEE Transactions on Power Delivery* 25(3) 1978–1985.

51. Das S, Chatterjee D and Goswami S K 2016 A GSA-based modified SVC switching scheme for load balancing and source power factor improvement. *IEEE Transactions on Power Delivery* 31(5) 2072–2082.